Proceedings of the 11th International Conference on Fluid Flow, Heat and Mass Transfer (FFHMT 2024)
Chestnut Conference Centre - University of Toronto, Toronto, Canada – June 16-18, 2024
Paper No. 104
DOI: 10.11159/ffhmt24.104

The Impact of the Incoming Non-Equilibrium Flow on the Hypersonic Wind Tunnel Heat Flux Prediction of A Re-Entry Body

Odelma Teixeira[1], José Páscoa[2]
[1,2]Center for Mechanical and Aerospace Science and Technologies
Universidade da Beira Interior,
6201-001, Covilhã, Portugal

Abstract – In this work, a numerical investigation of the vibrational non-equilibrium effects on the surface heat flux predictions of a re-entry body in hypersonic wind tunnels is performed. For this purpose, air mixture with five neutral species (N2, O2, NO, N and O) resulting from a 23.8 MJ/kg flow expansion from a plasma wind tunnel is considered to pass around a double-cone geometry. Non-equilibrium Navier-Stokes-Fourier equations within a density-based algorithm is here employed in the OpenFOAM framework. The numerical model was validated using data from experimental tests carried out at LENS-XX Expansion Tunnel facility and from past numerical results and proved to be very accurate with an excellent agreement with the experiments in terms of the size of the separation zone and an improvement of the heat flux peak value in 11% in comparison with past numerical results. It was found that when the freestream is in vibrational non-equilibrium, the shock waves/boundary layer interactions that occur in the flow field are felt more strongly in the test body surface then when the freestream is in equilibrium, resulting in an increase on the surface peak heat flux of 5%. It was also found a decrease in the thermal shock layer for non-equilibrium freestream condition, leading to higher temperature gradients in the flow field and consequently higher heat fluxes at the body surface.

***Keywords*:** Hypersonic Flow, Heat Flux, Thermochemical Non-equilibrium, Wind Tunnel, Re-entry Body, CFD

1. Introduction

In hypersonic wind tunnels, the flow, usually in high temperature and high pressure, is expanded through a converging-diverging nozzle, reaching very high Mach numbers at the nozzle exit and test chamber, where the studied test body is placed. In this way, it is possible to simulate the flight conditions experienced by a spacecraft during the atmospheric re-entry and have a better understanding of the complex phenomena occurring around the spacecraft [1]. During the expansion of the flow through the nozzle, the translation and rotational energy modes drop abruptly while the vibrational and electronic energies remain higher, at a temperature that is closer to the nozzle stagnation temperature. This cause the fluid to experience a non-equilibrium condition and change the quality of the flow at the test chamber [2]. In real flights, the vibrational excitation of the molecules is caused by the shock waves that form in front of the re-entry vehicle and the freestream is in equilibrium, while in hypersonic wind tunnels the molecules at the freestream are already vibrationally excited before the shock occur.

In this work, an investigation of the impact of the incoming vibrational non-equilibrium flow on the surface heat flux prediction of a re-entry body will be performed. For this purpose, the flow around a double-cone object, very used in the numerical investigation of shock waves/boundary layer interactions in hypersonic flight [3]–[8] will be considered. A high enthalpy flow of 23.8 MJ/kg will be studied by using computational fluid dynamics in a partially dissociated air composed by five neutral species (N_2, O_2, NO, N and O) with the freestream in equilibrium and vibrational non-equilibrium. A two-temperature finite volume density-based model [1], [2], [9] to solve non-equilibrium hypersonic nozzle flows and external aerodynamics in re-entry bodies will be here employed.

In the next sections, the governing equations and numerical methods are described, followed by the code validation and discussion of the results. Finally, the conclusions and further considerations are made.

2. Methodology

2.1. Governing Equations

The non-equilibrium Navier–Stokes–Fourier equations are here applied according to Park's two temperature model for thermal non-equilibrium [10]. The system of equations in the Cartesian coordinate is written as:

$$\frac{\partial \boldsymbol{U}}{\partial t} + \frac{\partial \left(\boldsymbol{F}_{i,inv} - \boldsymbol{F}_{i,vis} \right)}{\partial x_i} = \dot{\boldsymbol{W}} \tag{1}$$

where $\boldsymbol{F}_{i,in}$ and $\boldsymbol{F}_{i,vis}$ are the inviscid and viscous flux vectors respectively, $\dot{\boldsymbol{W}}$ is the source term vector and **U** is the vector of conserved quantities defined as

$$\boldsymbol{U} = \{\rho, \rho_s, \rho u, \rho v, \rho w, E_{ve,m}, E\}^T \quad s \in N_s, \quad m \in N_m \tag{2}$$

u, *v*, and *w* are the components of the velocity vector, ρ is the mass density of the fluid and ρ_s is the partial density of species s. E and $E_{ve,m}$ are the total energy and the total vibro-electronic energy for the molecule m, respectively. The source term is expressed by the vector:

$$\dot{\boldsymbol{W}} = \left(0, \dot{w}_s, 0,0,0, \dot{w}_{v,m}, 0\right)^T \tag{3}$$

where $\dot{w}_s$ represents the net mass production of species s and $\dot{w}_{v,m}$ is the vibrational source term calculated using the Landau-Teller equation [11] with the relaxation times obtained by Millikan-White formula [12] with Park's correction [13].

2.2. Numerical methods

The governing equations are solved using the finite volume density-based algorithm in the OpenFOAM software. The inviscid fluxes were discretized using second-order accurate central-upwing interpolations of Kurganov, Noelle and Petrova (KNP) [14], [15] with the second-order accuracy achieved using total variation diminishing (TVD) scheme with van Leer limiter function. The viscous fluxes were discretized using second-order central difference scheme. Euler discretization scheme with first-order accuracy is used for the temporal derivatives. The simulation is initialized using the freestream conditions and run until convergence to the steady state. The transport properties of the species are computed using Blottner's and Eucken's formulae [16], [17] and the mixture properties are obtained according to Wilke's mixing rule [18]. The diffusion flux is obtained using modified Fick's law [19] and the Park'93 model [20] is used for the chemical reactions. At the walls, no-slip boundary conditions were applied to the velocity and the temperature was set to 300 K. At the outlet, supersonic boundary condition was employed, with the field values being extrapolated from the domain.

3. Code Validation

As proved by Druguet at al. [21], the flow past a double-cone geometry is an excellent test case for assessing the accuracy of numerical methods for the compressible Navier-Stokes equations. Thus, freestream conditions with stagnation enthalpy of 5.44 MJ/kg and Mach number of 12.2 are here considered for the double cone geometry. Comparison of the present numerical results with the experimental data, carried out at LENS-XX Expansion Tunnel facility at Calspan-University of Buffalo Research Center by Holden et al. [22], and numerical results conducted by Hao and Wen [3] is performed. The fluid corresponds to a two-species gas mixture composed by molecular oxygen (O_2) and molecular nitrogen (N_2) with mass fractions of 0.235 and 0.765, respectively. A grid convergence analysis, showed that a grid with 512 and 265 cells along the wall and outlet, respectively, is sufficient to guarantee the independence of the results. The geometric dimensions of the double cone test used at LENS XX expansion tunnel and the computational domain with the grid and the boundary conditions used in the present numerical simulations are described in the Figure 1. The freestream conditions correspond to the experimental conditions of the Case A of Holden experiments, see Ref. [22].

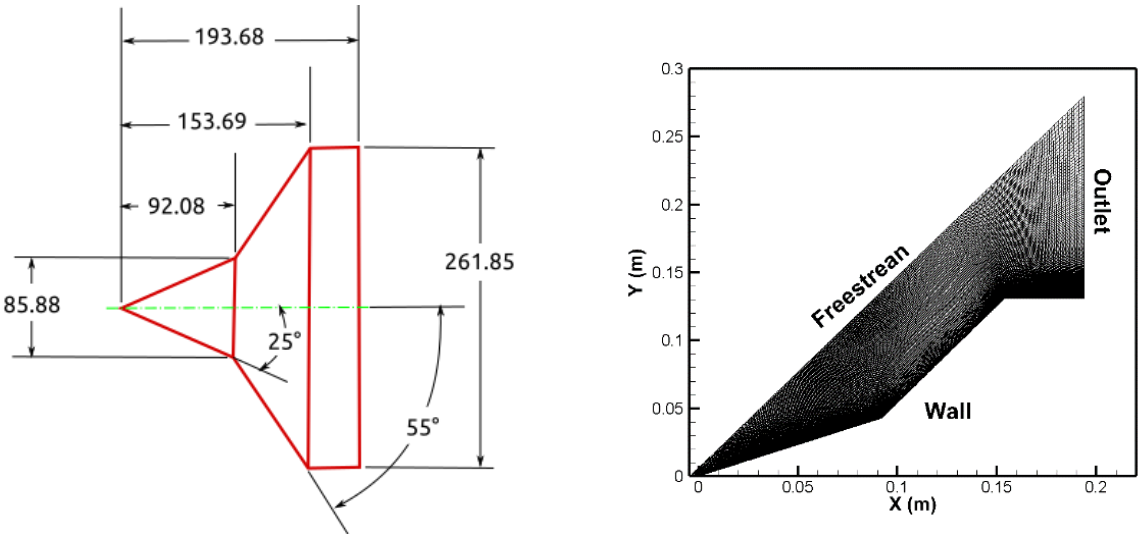

Figure 1 - Double cone geometry, dimensions in mm (left) and computational domain used in the CFD simulation (right).

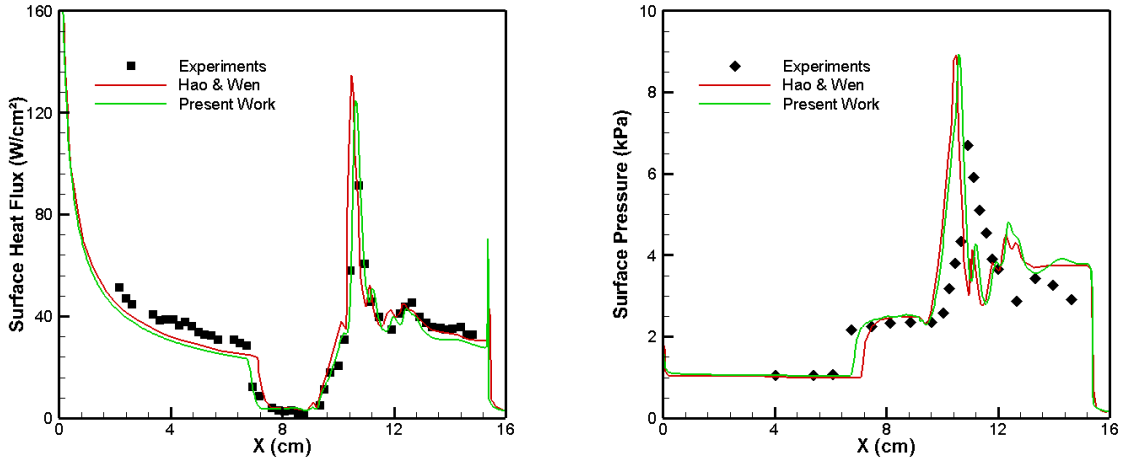

Figure 2 - Surface heat flux and pressure distribution. Comparison between Present Work, Experiments and Hao and Wen work.

Figure 2 shows the heat flux and pressure distribution along the double-cone surface and the comparison with experimental data [22] and numerical results [3]. As it can be seen, compared to Hao and Wen, the solution of the Present Work improves the results in terms of the size of the separation zone (near X = 7 cm), with an excellent agreement with the experiment. Additionally, the peak value for the heat flux, near X = 10 cm, is better predicted in the Present Work in comparison with Hao and Wen model, both considering Park's two temperature model with a mixture of perfect gases with vibrational non-equilibrium of single mode. It was verified an improvement of 11% on the heat flux peak value with the Present Work in comparison to the Hao and Wen work. Furthermore, a better alignment of the surface heat flux and surface pressure peak point with the experiments is observed in the present work. Thus, the present numerical model is demonstrated to be reliable and suitable to be used in this investigation.

4. Results

In order to understand the impact of the incoming vibrational non-equilibrium flow on the surface heat flux prediction of a re-entry body, numerical simulations were performed with thermal equilibrium and non-equilibrium conditions. The non-equilibrium freestream condition was taken from the numerical simulation of an expanded flow at the exit of the

hypersonic SCIROCCO Plasma wind tunnel convergent-divergent nozzle D, with 75 mm of throat diameter and an expansion ratio at the exit of 236 [2]. The equilibrium condition is also taken from the numerical simulation of the same nozzle, but in this case considering the expansion of the flow occurring in thermal equilibrium. The high stagnation enthalpy at the nozzle inlet causes the flow to be partially dissociated, resulting in a chemical non-equilibrium condition in the nozzle exit and in the freestream. In real flight, the freestream is in chemical equilibrium, but here to have an accurate relation on how the vibrational non-equilibrium impacts the heat flux predictions, the chemical non-equilibrium in the freestream will be considered in both situations. Table 1 describes the freestream conditions, trans-rotational temperature (T_{tr}), vibro-electronic temperature (T_{ve}), pressure and velocity, used in the simulations. Table 2 shows the species composition in the freestream, in terms of mass fraction, for equilibrium and non-equilibrium conditions. The double-cone geometry and computational domain are consistent with the represented in the Figure 1.

Table 1 – Vibrational equilibrium and non-equilibrium freestream conditions.

	T_{tr} (K)	T_{ve} (K)	Pressure (Pa)	Velocity (m/s)
Equilibrium	604	604	17.00	5094
Non-equilibrium	509	3314	14.87	5115

Table 2 – Species mass fraction at the freestream.

	N_2	O_2	N	O	NO
Equilibrium	0.574998	8.05e-07	0.196	0.229	1.67e-06
Non-equilibrium	0.574997	1.62e-09	0.196	0.229	2.8e-06

Figure 3 shows the heat flux and pressure distribution at the double-cone surface for equilibrium and non-equilibrium freestream conditions. It is possible to observe that for the first cone, from X = 0 cm to X = 9.2 cm, the heat flux distribution is almost coincident for both conditions. From the beginning of the second cone, the heat flux starts to grow more rapidly for the non-equilibrium freestream condition, reaching a higher peak value at around 10 cm. After this point the heat flux starts to decrease in a similar rate, with the values for the non-equilibrium condition being slightly higher along the second cone. For the surface pressure, the results with the non-equilibrium condition starts to be slightly higher than the equilibrium condition since the beginning of the first cone, however, the relevant difference also starts at the beginning of the second cone, reaching the peak value also around the same position of the heat flux peak point and decreasing after that, being higher for the non-equilibrium condition along the remaining part of the second cone. From Figure 4 it is possible to understand why the surface heat flux and the surface pressure reaches a peak value at the second cone, around X = 10 cm. As can be seen from the pressure and Mach number contours, around 10 cm is where the oblique shock formed by the first cone and the detached shock formed by the second cone are impinged to the second cone surface and interact with the boundary. These interactions cause the abrupt increase on the heat flux verified in the second cone surface.

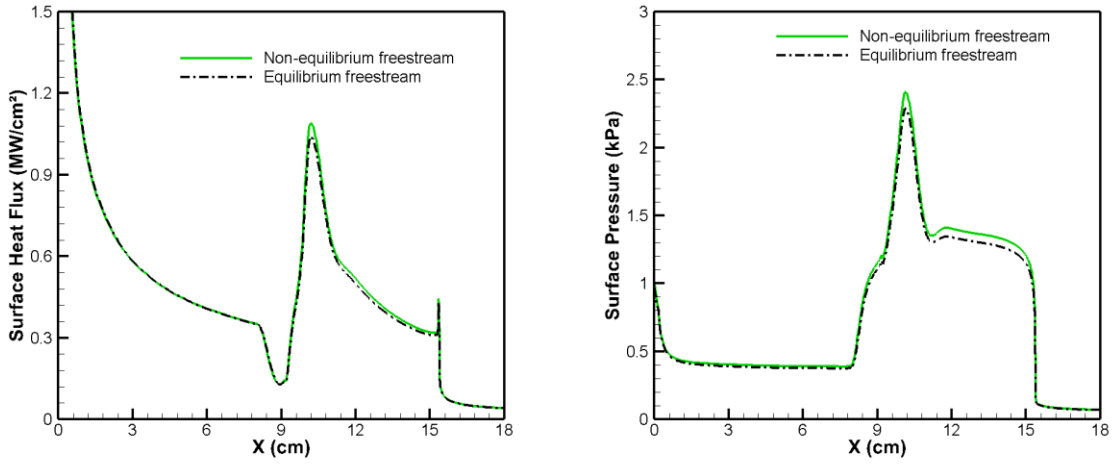

Figure 3 - Surface heat flux (left) and surface pressure (right) distribution for equilibrium and non-equilibrium freestream.

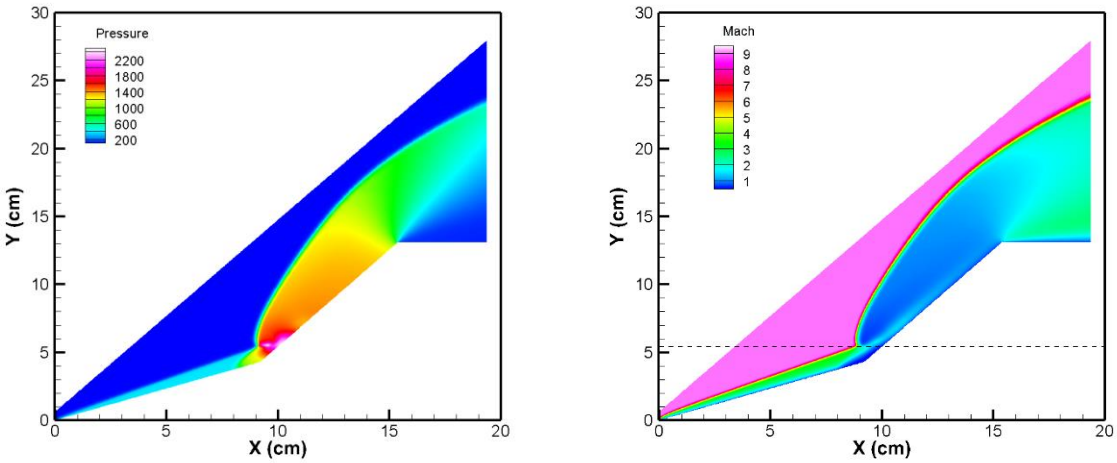

Figure 4 - Static pressure (left) and Mach number contour (right) for the non-equilibrium freestream condition.

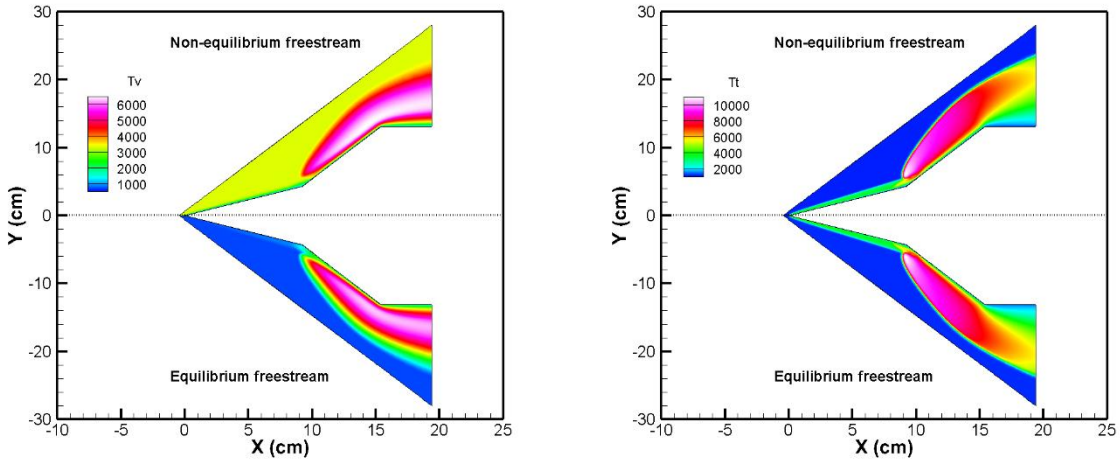

Figure 5 – Vibro-electronic temperature (left) and trans-rotational temperature contour (right) for equilibrium and non-equilibrium freestream.

Figure 5 shows the vibro-electronic (left) and trans-rotational temperature (right) contours for equilibrium and non-equilibrium freestream conditions. It is clear, how the presence of vibrational non-equilibrium in the freestream alters the vibro-electronic temperature distribution in the flow field, more specifically around the second cone. For the trans-rotational temperature, the flow contours look very similar for both conditions, so that, a plot along the line Y= 5.42 cm, horizontal dashed line highlighted at Figure 4 (right), starting from the freestream to the second cone at X = 10 cm is drawn in order to understand the temperature difference between both conditions in more details, Figure 6.

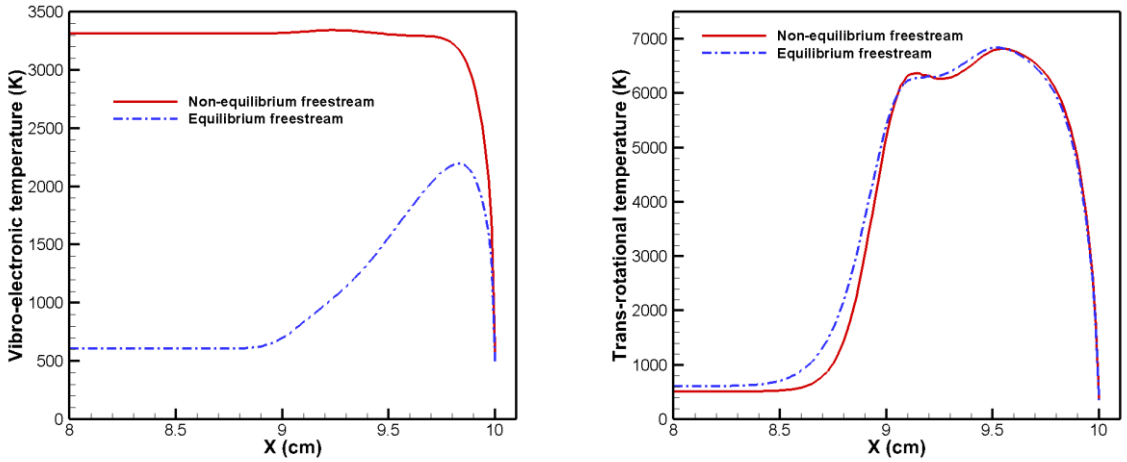

Figure 6 – Vibro-electronic temperature (left) and trans-rotational temperature (right) distribution along the line Y = 5.42 cm.

As it can be seen, that is a very high gradient of vibro-electronic temperature for non-equilibrium condition compared to the situation where the freestream is in equilibrium. This greater gradient of temperature is one of the reasons for the higher heat flux peak value that was observed at X = 10 cm for vibrational non-equilibrium. For the trans-rotational temperature, the contribution for the heat flux is smaller in terms of the temperature gradient near the second cone surface, however, the thermal shock layer formed by the detached shock is thinner for the non-equilibrium freestream condition, indicating that the flow would experience higher temperature gradients inside the shock, which will also contribute to the increment of the heat flux at the cone surface.

5. Conclusion

Motivated by the extreme importance of wind tunnels in the hypersonic research, especially in the design and qualification of thermal protection systems for re-entry vehicles, in this paper, a numerical investigation of the impact of the incoming vibrational non-equilibrium flow, resulting from the expansion of the flow through a hypersonic wind tunnel nozzle, in a re-entry vehicle heat flux prediction is performed. A 23.8 MJ/kg expanded flow composed by a 5-species partially dissociated air mixture around a double-cone body is simulated using Navier-Stokes-Fourier equations according to Park's two temperature model for equilibrium and non-equilibrium freestream conditions. The main conclusions are summarised as follows.

- The vibrational non-equilibrium freestream conditions increase the temperature gradient in the flow field.
- The thermal shock layer is thinner for the non-equilibrium freestream condition.
- The pressure along the body surface is higher for the non-equilibrium freestream condition, indicating stronger shock waves/boundary layer interactions.
- All the aspects mentioned above contribute to the higher surface heat flux observed for the non-equilibrium freestream, particularly at the surface region where the interaction between the shock waves and the boundary layer is felt.

After this investigation, we can conclude that due to the vibrational non equilibrium, the heat flux in a re-entry body surface predicted in hypersonic wind tunnel experiments is higher than the real flight values. In this study, the predicted peak value was found to be 5% greater than the value expected in the real flight.

Acknowledgements

This research was funded by the Portuguese Foundation for Science and Technology, I.P. (FCT, I.P.) FCT/MCTES through national funds (PIDDAC), under the R&D Unit C-MAST/Center for Mechanical and Aerospace Science and Technologies, reference: Projects UIDB/00151/2020 (https://doi.org/10.54499/UIDB/00151/2020) and UIDP/00151/2020 (https://doi.org/10.54499/UIDP/00151/2020).

References

[1] O. Teixeira and J. Pascoa, "Computational Modelling of Hypersonic Nozzles: The Influence of Enthalpy on the Flow Thermochemistry," in AeroTech Conference & Exhibition, Charlotte, NC, USA, Mar. 2024.

[2] O. Teixeira and J. Páscoa, "Catalytic wall effects for hypersonic nozzle flow in thermochemical non-equilibrium," Acta Astronaut., vol. 203, pp. 48–59, Feb. 2023.

[3] J. Hao and C. Y. Wen, "Effects of vibrational nonequilibrium on hypersonic shock-wave/laminar boundary-layer interactions," Int. Commun. Heat Mass Transf., vol. 97, no. August, pp. 136–142, 2018.

[4] N. Kianvashrad and D. D. Knight, "The Effect of Thermochemistry on Prediction of Aerothermodynamic Loading over a Double Cone in a Laminar Hypersonic Flow," in 2018 AIAA Aerospace Sciences Meeting, 2018.

[5] J. Hao, J. Wang, and C. Lee, "Numerical Simulation of High-Enthalpy Double-Cone Flows," AIAA J., vol. 55, no. 7, pp. 2471–2475, Jul. 2017.

[6] K. Vogiatzis, E. Josyula, and P. Vedula, "Double-Cone Flows in Nonequilibrium: Comparison of CFD with Experimental Data," in 55th AIAA Aerospace Sciences Meeting, 2017.

[7] G. V. Candler, "Next-Generation CFD for Hypersonic and Aerothermal Flows (Invited)," in 22nd AIAA Computational Fluid Dynamics Conference, 2015.

[8] I. Nompelis and G. V. Candler, "US3D Predictions of Double-Cone and Hollow Cylinder-Flare Flows at High-Enthalpy (Invited)," in 44th AIAA Fluid Dynamics Conference, 2014.

[9] O. Teixeira and J. Pascoa, "Hypersonic Flow Simulation towards Space Propulsion Geometries," SAE Int. J. Adv. Curr. Pract. Mobil., vol. 2, no. 2, pp. 803–810, 2020.

[10] C. Park, "Two-temperature interpretation of dissociation rate data for N2 and O2," in 26th Aerospace Sciences Meeting, 1988.

[11] L. Landau and E. Teller, "On the Theory of Sound Dispersion," Phys. Zeitschrift der Sowjetunion, vol. 10, no. 34, pp. 147–153, 1936.

[12] R. C. Millikan and D. R. White, “Systematics of Vibrational Relaxation,” J. Chem. Phys., vol. 39, no. 12, pp. 3209–3213, Dec. 1963.
[13] C. Park, Nonequilibrium Hypersonic Aerothermodynamics. New York: Wiley International, 1990.
[14] C. J. Greenshields, H. G. Weller, L. Gasparini, and J. M. Reese, “Implementation of semi-discrete, non-staggered central schemes in a colocated, polyhedral, finite volume framework, for high-speed viscous flows,” Int. J. Numer. Methods Fluids, vol. 63, no. 1, pp. 1–21, 2010.
[15] A. Kurganov, S. Noelle, and G. Petrova, “Semidiscrete Central-Upwind Schemes for Hyperbolic Conservation Laws and Hamilton--Jacobi Equations,” SIAM J. Sci. Comput., vol. 23, no. 3, pp. 707–740, Jan. 2001.
[16] F. G. Blottner, M. Johnson, and M. Ellis, “Chemically Reacting Viscous Flow Program for Multi-Component Gas Mixtures.,” Albuquerque, NM, and Livermore, CA (United States), Jan. 1971.
[17] V. Casseau, “An Open-Source CFD Solver for Planetary Entry,” University of Strathclyde, 2017.
[18] C. R. Wilke, “A Viscosity Equation for Gas Mixtures,” J. Chem. Phys., vol. 18, no. 4, pp. 517–519, Apr. 1950.
[19] K. Sutton and P. Gnoffo, “Multi-component diffusion with application to computational aerothermodynamics,” in 7th AIAA/ASME Joint Thermophysics and Heat Transfer Conference, 1998.
[20] C. Park, “Review of chemical-kinetic problems of future NASA missions. I - Earth entries,” J. Thermophys. Heat Transf., vol. 7, no. 3, pp. 385–398, Jul. 1993.
[21] M.-C. Druguet, G. V. Candler, and I. Nompelis, “Effects of Numerics on Navier-Stokes Computations of Hypersonic Double-Cone Flows,” AIAA J., vol. 43, no. 3, pp. 616–623, Mar. 2005.
[22] M. S. Holden, T. P. Wadhams, M. G. MacLean, and A. T. Dufrene, “Measurements of Real Gas Effects on Regions of Laminar Shock Wave/Boundary Layer Interaction in Hypervelocity Flows for “Blind’ Code Validation Studies,” 21st AIAA Comput. Fluid Dyn. Conf., pp. 1–13, 2013.